Article

High-Altitude Operation of a Commercial 100 kW PEM Fuel Cell System

Caroline Willich *[ID], Daniel Frank [ID], Tobias Graf [ID], Stefan Wazlawik [ID], Samara Brandao and Christiane Bauer [ID]

Institute for Energy Conversion and Storage, Ulm University, Albert-Einstein-Allee 47, 89081 Ulm, Germany; daniel.frank@uni-ulm.de (D.F.); tobias-1.graf@uni-ulm.de (T.G.); stefan.wazlawik@uni-ulm.de (S.W.); samara.brandao@uni-ulm.de (S.B.); christiane.bauer@uni-ulm.de (C.B.)
* Correspondence: caroline.willich@uni-ulm.de

Abstract: A commercially available 100 kW PEM fuel cell system designed for efficient operation on ground-level was tested at low ambient pressures between 750 mbar and 940 mbar in a low-pressure chamber. The current–voltage characteristics at 940 mbar and 900 mbar showed only small differences, while the system performed worse at lower ambient pressures. To enable operation at these low pressures, an additional current-limiting strategy had to be implemented, as it was found that the compressor could not deliver sufficient mass flow at ambient pressures below 867 mbar to reach the maximum current allowed by the system (420 A). The results show that the fuel cell system, which was designed for ground-level applications, can be operated at lower pressures if the proposed current-limiting strategy is implemented, although at the cost of a lower maximum current output at low ambient pressures. Based on the results, suggestions for further hardware measures to optimise the system for flight conditions are made.

Keywords: PEM fuel cell system; aviation; low pressure; altitude; mass flow limitation; stoichiometry control; ground-to-aviation adaption

1. Introduction

Hydrogen powered aircraft have the potential to significantly reduce the climate impact of aviation [1]. The conversion in fuel cells offers higher efficiencies compared to combustion engines or turbines. Fuel cell (FC) systems are already commercially available for applications on ground. However, the operation at high altitudes requires modifications to existing systems. Despite the growing interest and many ongoing activities by several companies, like H2Fly [2], ZeroAvia [3] or Airbus [4], as well as research institutions, commercial fuel cell systems optimised for aviation are not yet available. Several stack and fuel cell system manufacturers are working on the adaptation of their ground level systems, but no commercial fuel cell system optimised for flight is yet being offered. There is also little information available in the literature about the necessary adaptations on system level.

Proton exchange membrane (PEM) fuel cells require a complex balance of plant to achieve optimal operation [5–7]. An exemplary system layout can be observed in Figure 1, although other configurations are possible as well. The hydrogen supply has to be controlled via valves, pumps and pressure regulators, and the ambient air needs to be conditioned. It is filtered to reduce contamination. In pressurised systems, a compressor then compresses the air. Due to the compression, the air temperature increases, and a heat exchanger is necessary to obtain a suitable inlet temperature for the fuel cell. A humidifier increases the water content of the inlet air to avoid drying out the fuel cell.
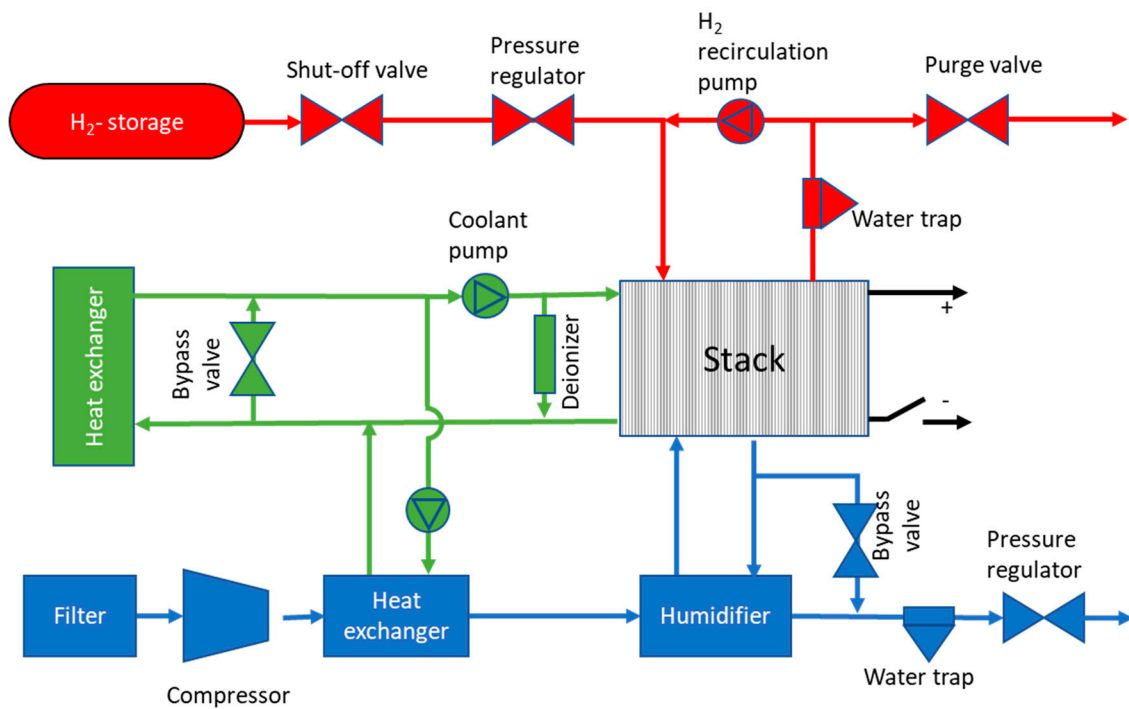
Figure 1. Exemplary schematic of a PEM fuel cell system. Other configurations are possible as well.

It is well known that the performance of fuel cells is influenced by the operational pressure. Higher pressures increase the performance and efficiency. At high altitudes of approximately 10,000 m at which commercial aircraft fly, the ambient pressure is only approximately 250 mbar, meaning that air-breathing fuel cells will have to operate at these pressures. Low pressures reduce the efficiency and performance of PEM fuel cells. The open circuit voltage of a fuel cell changes with pressure according to the Nernst equation. It depends on the gas composition and increases with higher pressures [8]. Low ambient pressures will decrease it. It has been shown that the operational pressure also has an influence on the activation overpotentials of the cells. The reason is that, due to higher partial pressures, more reactants adsorb on the active sites of the electrodes, increasing the charge transfer reaction and the exchange current density [9]. It is, therefore, to be expected that, at low pressures, the charge transfer reaction will slow down due to a lower surface coverage. The concentration overpotentials in a fuel cell are also influenced by pressure. These are dominated by diffusion processes due to concentration gradients. The concentration gradient within the fuel cell itself as well as the effective diffusion coefficient are pressure dependent, and lower pressures are expected to lead to higher diffusion overpotentials [10]. In PEM fuel cells, pressure can indirectly influence the ohmic overpotential since the resistance of the membrane is related to the humidity. The dew point of water changes with pressure [11], and lower operating pressures will lead to a change in the water management of the cell. At a fixed temperature, the air will be drier at a lower operating pressure, which reduces the H^+-ion conductivity of the membrane and, therefore, increases the ohmic loss [12]. Werner et al. [12,13] found a decrease in overall stack performance and efficiency of 5.3% when they reduced the operating pressure from 950 to 700 mbar. They also examined how the operating temperature of the fuel cell should be adapted at low pressures to maximise power output. The operating conditions in aviation, however, will reach even lower pressures down to 250 mbar.

The decreasing performance of fuel cells at low pressures can be mitigated by pressurising the air with the help of a compressor. Most current developments and research activities use centrifugal compressors for supplying the fuel cell with air [14–17]. The fuel cell is influenced by low ambient pressures, and the absolute outlet pressure as well as the mass flow, which can be delivered by a centrifugal compressor, also change with the inlet

pressure. It has been shown previously that a change in the ambient pressure leads to a shift in the compressor operational map of centrifugal compressors [18], as can be observed in Figure 2. The operational map of a centrifugal compressor is limited towards the left by the surge line. The surge limit defines the minimal flow through the compressor at a certain pressure level due to aerodynamic limitations. At the surge limit, the flow through the compressor stalls. If this line is crossed, fluid can flow backwards through the compressor, leading to an unstable operation. This leads to strong mass flow and pressure oscillations and forces on the blades and shaft, which can lead to severe damages [19], especially in compressors with air bearings. At the choke limit, the fluid passing through the compressor reaches the speed of sound in any part of the compressor [20]. It can then no longer be accelerated further, and it is impossible to increase the mass flow further at that pressure level. As the speed of sound in an ideal gas depends on pressure, temperature and density, the choke limit is, therefore, influenced by any change in inlet conditions. The rotational speed of a compressor is also limited due to structural and material considerations. This speed limit is implemented in the inverter control in an electric centrifugal compressor in order to avoid damages to the compressor.
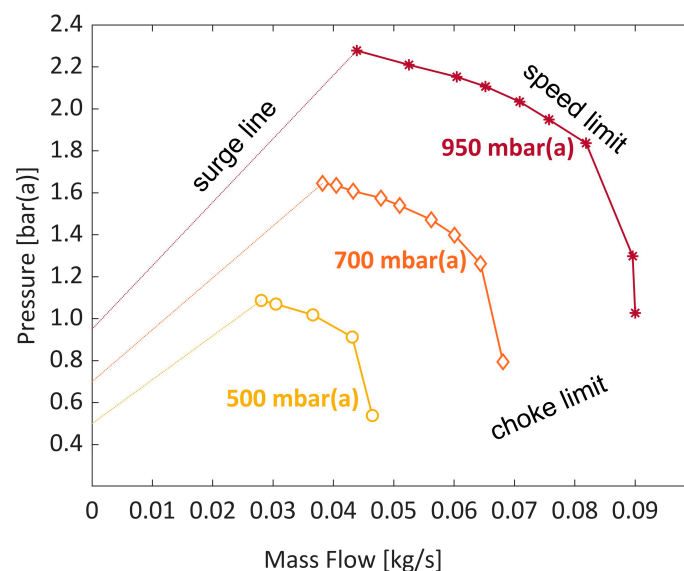

Figure 2. Exemplary compressor operational maps at different inlet pressures based on data of a Rotrex EK10AA (Rotrex A/S, DK) from [18]. Maximum compressor speed: 140 krpm; inlet temperature: 20 °C.

All balance of plant components must work together to optimise the performance of the fuel cell. A change in the behaviour of one component has an effect on all the others. In this contribution, a commercially available fuel cell system, which is designed and built for ground application, was tested at lower-than-sea-level ambient pressures down to 750 mbar, and the results were analysed to point out and demonstrate system aspects that require modification in hard- or software when operating the system at high altitudes.

2. Experimental Setup

For the characterisation of the fuel cell system at various ambient pressures, a low-pressure climate chamber [21] was used. The chamber makes it possible to measure at defined ambient conditions. For the here presented work, measurements within a pressure range of 0.75 to 0.94 bar were performed. A continuous air mass flow through the chamber of up to 600 m^3/h allows for the operation of a fuel cell system inside, which takes its air supply from inside the chamber.

A commercially available fuel cell system (PS-100, PowerCell Sweden AB, Gothenburg, Sweden, SWE), which was customised to allow for greater access to the air supply part of

the system, with a nominal power output of 100 kW [22] was set up inside the low-pressure chamber and equipped with the necessary periphery for H_2 and air supply, high voltage (HV) and low voltage (LV) connections, cooling as well as additional sensors, as is shown schematically in Figures 3 and 4.
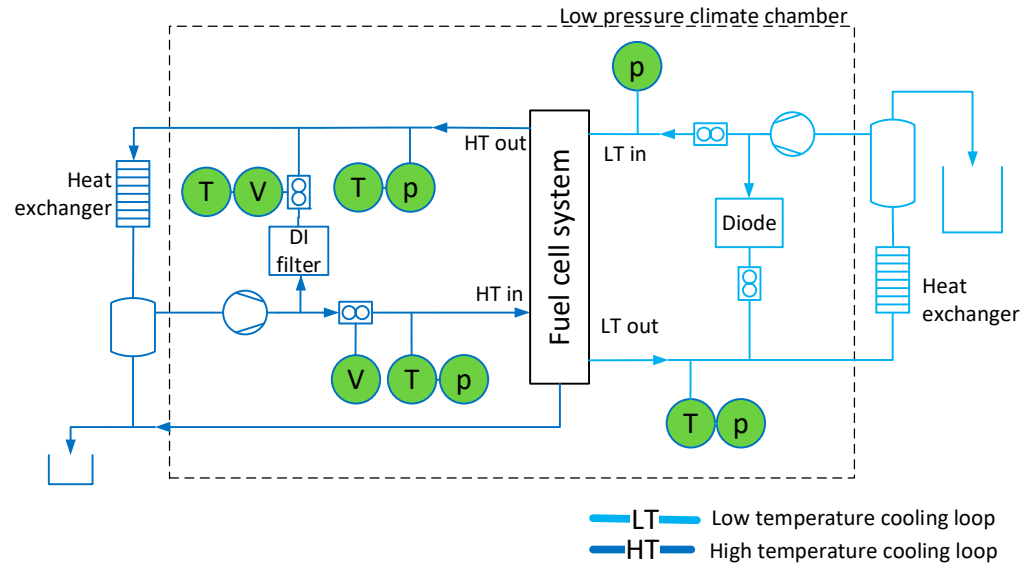

Figure 3. Layout of high (HT)- and low (LT)-temperature cooling system for the fuel cell system test rig with deionising filter (DI) and sensors for pressure (p), temperature (T) and volume (V).
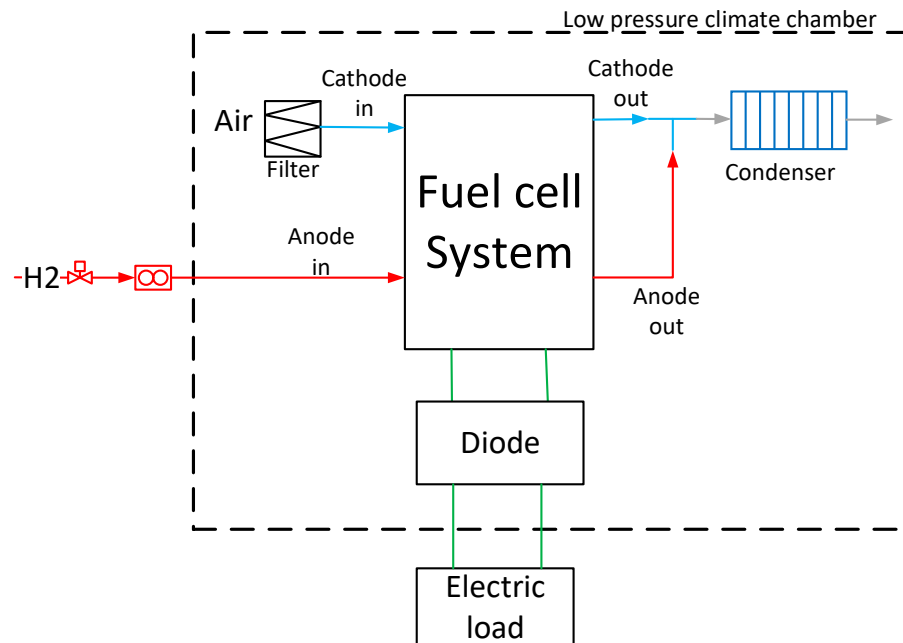
Figure 4. Layout of the hydrogen (in red) and air (in blue) supply as well as the electrical HV connection (in green) for the fuel cell system test rig.

Data for stack voltage and current, compressor speed and power as well as cathode air mass flow and pressure are obtained via the internal sensors of the fuel cell system. The temperatures of the high-temperature (HT) cooling loop at the inlet and outlet of the system were measured using sensors, type TM5101 (IFM electronic GmbH, Essen, Germany, GER), with a measurement accuracy of ±0.15 K + 0.002x measurement value. Inside the low-pressure chamber, temperature was measured using a sensor by a PT100 Form F (Jumo GmbH & Co. KG, Fulda, Germany, GER), with a measurement accuracy of ±0.3 K + 0.005x

measurement value. The pressure inside the chamber was obtained using a sensor by Endress+Hauser Inc. (Reinach, Switzerland, GER), with a nominal measurement accuracy of 1% of the measurement range.

The fuel cell system has its own internal control, but a control software for the test rig using LabView Professional Development System, Version 21.0.1f1 (32 bit) by National Instruments (Austin, TX, USA) and CANoe Version 17.3.91 (SP3) (64 bit) by Vector Informatik GmbH (Stuttgart, Germany, GER) for testing, data acquisition, monitoring and error management was implemented. The software ensures that no limiting parameters are exceeded and transfers the system into a safe state should any difficulties arise. The fuel cell system cannot be operated at ambient pressures below 700 mbar due to the compressor's air bearings. Operation at lower pressures will lead to severe damage of the compressor. Lower pressures can, therefore, not be examined without a change in hardware.

The 24 V supply of the system, which mainly supplies the cooling pumps but also some sensors and controllers, is treated as negligible in the following considerations, since the major auxiliary power demand is that of the air compressor.

3. Sensitivity of the Measured Data to Deviation in Environmental Conditions

To assess the susceptibility of the system to external experimental parameters, several preliminary tests were performed.

3.1. Sensitivity to System Cooling Inlet Temperature

The influence of system coolant temperatures of the high-temperature cooling loop was estimated through tests where the system coolant inlet temperature to the fuel cell system was set to 20 °C, 40 °C and 60 °C, and the fuel cell system was operated at currents of 100 A, 200 A, 400 A and 420 A at 900 mbar and 15 °C ambient temperature.

The tests were repeated on different days. From these measurements, it was concluded that the impact of the HT cooling system inlet temperature (marked as "HT in" in Figure 3) is negligible, as the difference between measurements on day 1 and 2 showed a larger influence than the variation in the coolant temperature. The average cell voltage at 400 A varied up to 19 mV for the measurements at different days, while variation due to the system coolant inlet temperature was below 10 mV at the same current.

The fuel cell system has an internal control of the stack cooling, which is a black box system to the user. Higher coolant flows proved to be preferable for the examined setup, as the flow sensor (Bürkert S030/SE35, Christian Bürkert GmbH & Co. KG, Ingelfingen, Germany) installed in the HT cooling loop has its lower measurement limit at 35 L/min. Too high temperatures in the HT cooling inlet should be avoided, also during controlling overshoots or load changes. The standard temperature of the HT cooling inlet was, therefore, set to 50 °C ± 5 K for all further experiments.

3.2. Sensitivity to Ambient Pressure

To estimate the sensitivity of the fuel cell system to changes in the ambient pressure, the ambient pressure was varied from approximately 900 mbar to 790 mbar for loads of 250 A and the maximum possible current for each pressure. The maximum allowed current of 420 A could be drawn from the system only at ambient pressures higher than 865 mbar. For lower pressures, the current had to be reduced to meet a minimal target stoichiometry of $\lambda_{cath} = 1.7$.

For the estimation of the influence of the ambient pressure, constant loads of 250 A and 420 A (if possible) were considered, and linear fits of the mean cell voltage and stack power as functions of ambient pressure were calculated. The results showed a sensitivity of 0.14 mV/mbar or 0.016 kW/mbar at 250 A and 0.11 mV/mbar or 0.02 kW/mbar at 420 A.

Therefore, ambient pressures in future experiments were considered constant for pressure conditions in a range of ±5 mbar.

3.3. Sensitivity to Ambient Temperature

The cooling system should ensure a suitable operating temperature of the fuel cell stack in all operating conditions. To estimate the influence of the ambient temperature on the fuel cell system, the ambient temperature was varied (15 °C and 20 °C) for currents of 250 A and 420 A. For both current values, linear fits of the mean cell voltage and stack power as functions of the ambient pressure were calculated. The results showed a sensitivity of −0.38 mV/K or −0.039 kW/K at 250 A and 1.42 mV/K or 0.28 kW/K at 420 A and 900 mbar.

As the observed sensitivity had a reversed sign and was in absolute values lower by an order of magnitude for the 250 A measurement in comparison to the 420 A measurement, the influence of the ambient temperature at loads of 250 A was considered neglectable within the examined temperature range.

For the 420 A setpoint, a deviation in ambient temperature of 2 K resulted in a deviation of the measured stack power of approximately 0.5% of the nominal stack power. Ambient temperatures in the following experiments were, therefore, considered constant within a range of ± 2 K.

3.4. Reproducibility of Measurements

Several measurements of a reference I–V curve were taken before and after the experiments. The reference measurements were taken at 900 ± 5 mbar, ambient temperature of 15 ± 2 °C and a relative humidity of 50% inside the low-pressure climate chamber. The high-temperature cooling loop had a system inlet temperature of 50 ± 5 °C. Measurements were taken at currents of 45 A, 60 A, 75 A, 100 A, 125 A, 150 A, 200 A, 250 A, 300 A, 350 A, 375 A, 390 A, 400 A, 410 A and 420 A. Every point was held for at least 2 min and until the average cell voltage changed less than 0.6 mV/min. Figure 5 shows the averaged I–V curves from 4 of these reference measurements as well as the absolute error bars to show the reproducibility of the measurements. The maximum deviation between points at the same current was 4.65 V.
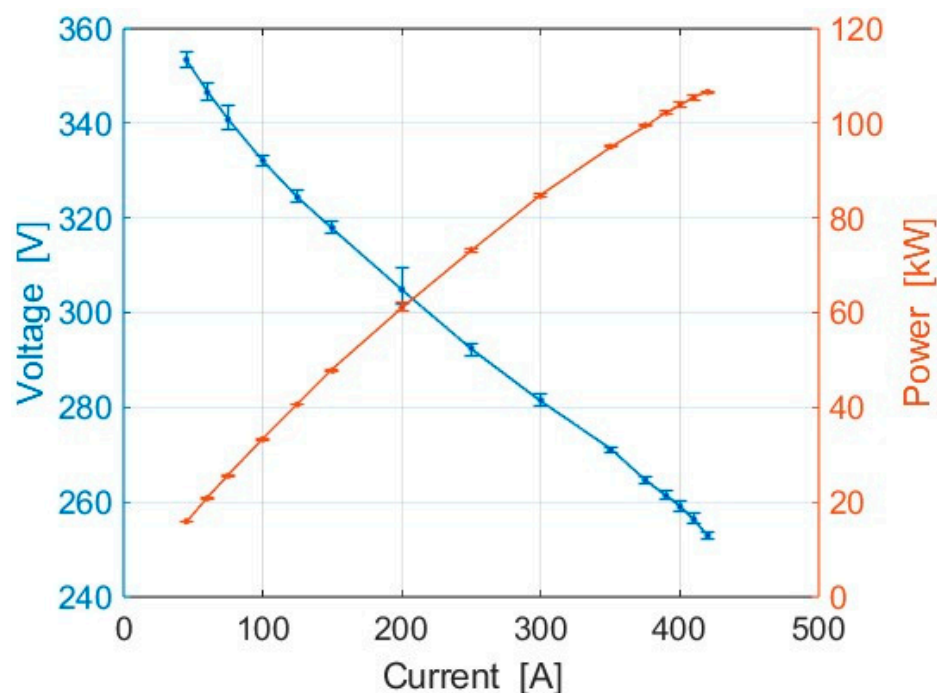

Figure 5. Averaged reference I–V curve and stack power from 4 single measurements with error bars.

4. Stoichiometry-Dependent Current Limiting

At low ambient pressures, the mass flow that the compressor can deliver decreases [18]. During initial operation, it was found that too low an air mass flow led to a hard shutdown

of the system. The conditions at which these shutdowns occurred for the examined system appeared to correlate to when the stoichiometry at the cathode fell below a threshold of approximately $\lambda_{Thres} = 1.55$. In these cases, the manufacturer's own system software effectively prevented oxygen starvation in the fuel cell by performing a hard shutdown of the system. The system was not designed for aviation applications, but a hard shutdown of the system at high load is especially undesirable in aviation, as maximum power conditions occur during take-off and climb, where a failure of the fuel cell system can have serious consequences. An unexpected shutdown can be fatal unless redundant propulsion systems can still ensure a safe landing. Low stoichiometry also leads to increased degradation, which should be avoided as well. With a focus on an adequate approach for flight applications, a method for avoiding a hard shutdown was developed, implemented and tested successfully on the test rig.

The method ensures that the stoichiometry is well above the observed threshold of $\lambda_{Thres} = 1.55$ at any given time by limiting the allowed current drawn from the fuel cell system. This procedure is essential to be able to carry out the laboratory tests with this FC-system at low pressures as they occur in flight applications.

During operation, the maximum current that can instantly be drawn from the FC-system $I_{max,Stoich}$ is calculated from the measured cathode air mass flow $\dot{m}_{air}$ and the minimal target stoichiometry λ_{min} using Faraday's law [23], as observed in Equation (1), where $n_{e^-,\ Cath}$ is the number of exchanged electrons on the cathode, F the Faraday constant, x_{O_2} the mol fraction of oxygen, M_{O_2} the molecular mass of oxygen and n_{Cells} the number of fuel cells in the stack. λ_{min} needs to be greater than the shutdown threshold λ_{Thres}, with a sufficient safety margin to avoid a hard shutdown due to fluctuations in the cathode mass flow or due to measurement noise. For all of the following experiments, this target was set to $\lambda_{min} = 1.7$.

$$
I_{max,Stoich} = \underbrace{\dot{m}_{air}}_{\text{measured}} \times \underbrace{\frac{1}{\lambda_{min}}}_{\text{defined by user}} \times \underbrace{\frac{n_{e^-,\ Cath} \times F \times x_{O_2}}{M_{O_2} \times n_{Cells}}}_{\text{constant}} \tag{1}
$$

During operation of the fuel cell system, $I_{max,Stoich}$ is calculated according to the current operating conditions.

When current is increased, the FC-system will react and increase the compressor speed and air mass flow $\dot{m}_{air}$, increasing the allowed current $I_{max,Stoich}$. Further ramp up of the current is possible at any time, as long as the λ_{min}-condition is met and the compressor is not at its speed limit of 120 krpm.

When the ambient pressure decreases at a constant current, the compressor speed must increase in order to maintain the cathode air mass flow. As the maximum compressor speed is limited, the cathode air mass flow will also reach a limit. If ambient pressure is further decreased, the current drawn from the fuel cell stack must also be reduced to the allowed current $I_{max,Stoich}$ according to Equation (1). $I_{max,Stoich}$ is, therefore, pressure dependent.

The FC-system itself determines a maximum allowed current $I_{max,\ Sys}$, depending on the state of the system, e.g., during start-up or at non-optimal cooling conditions, which, however, does not consider the pressure-dependent performance of the compressor. The maximum allowed current I_{max} is, therefore, the minimum of $I_{max,Stoich}$ and $I_{max,\ Sys}$ as shown in Equation (2):

$$
I_{max} = min\left(I_{max,Stoich}, I_{max,\ Sys}\right) \tag{2}
$$

This developed method now allows for the stable operation and testing of the commercial FC-system originally developed for automotive purposes, also at low ambient pressures.

Figure 6 shows the current limiting that prevents the hard shutdown due to oxygen starvation. During this measurement, the fuel cell was initially loaded with the maximum allowed current $I_{max,\ Sys} = 420$ A, and the ambient pressure p_0 was then successively lowered. Once the compressor had reached its speed limit, further lowering of p_0 decreased the stoichiometry, as can be observed in Figure 6, and eventually would have led to a

system shutdown with the standard configuration, as described above. With the newly developed method of current limiting, the shutdown was successfully prevented, as can be observed in Figure 6.
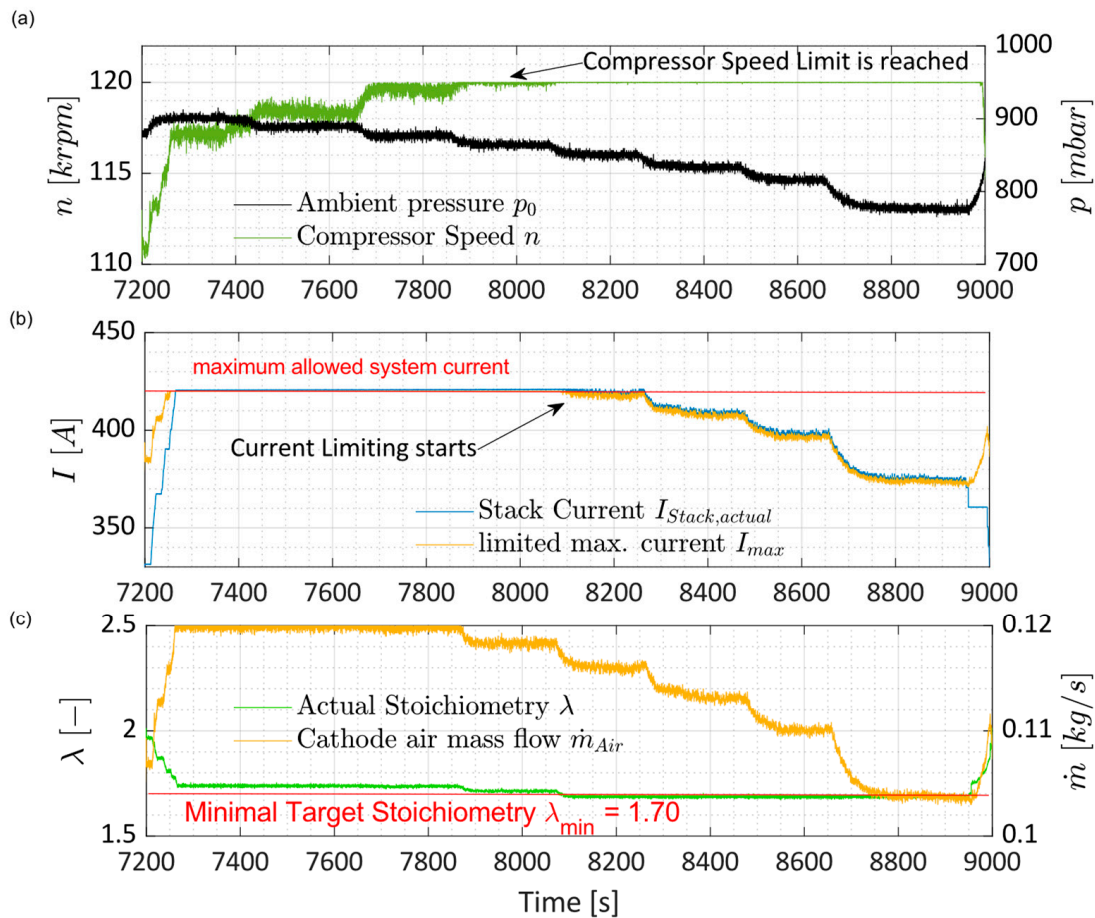

Figure 6. Measured data showing the current limiting at lower pressures to avoid shutdown of the system. (**a**) Compressor speed and ambient pressure; (**b**) fuel cell current; (**c**) cathode stoichiometry and air mass flow.

The stability of the current output can be improved further by introducing a filter on the mass flow signal, if found necessary. The proposed alteration to the system is purely a programming adaptation, which is fairly easily implemented and is not a significant cost factor. The current-limiting control strategy will prevent a hard shutdown due to lack of air at lower pressures. Neither does it prevent shutdowns due to other causes, nor does it prevent damage to the cell for any other causes than air starvation. A detailed failure analysis is not the focus of this work. Implementing the current-limiting strategy, however, made further measurements at low pressures possible.

5. Results

Measurements were performed at pressures of 940 mbar, 900 mbar, 845 mbar, 795 mbar and 750 mbar. The temperature inside the chamber was set to 15 °C for all measurements. The resulting current–voltage characteristics of the fuel cell system can be observed in Figure 7. Figure 7 also shows the inlet pressure of the air into the fuel cell stack, the fuel cell outlet temperature, compressor power and compressor speed, air mass flow and stoichiometry measured during the I–V curves at different ambient pressures.

When looking at the current–voltage characteristics at 940 mbar and at 900 mbar, the system behaves almost the same, and very little adverse effects of the lower pressure can be

observed. For lower pressures, however, the performance of the fuel cell system decreases, and the characteristic curves are steeper.
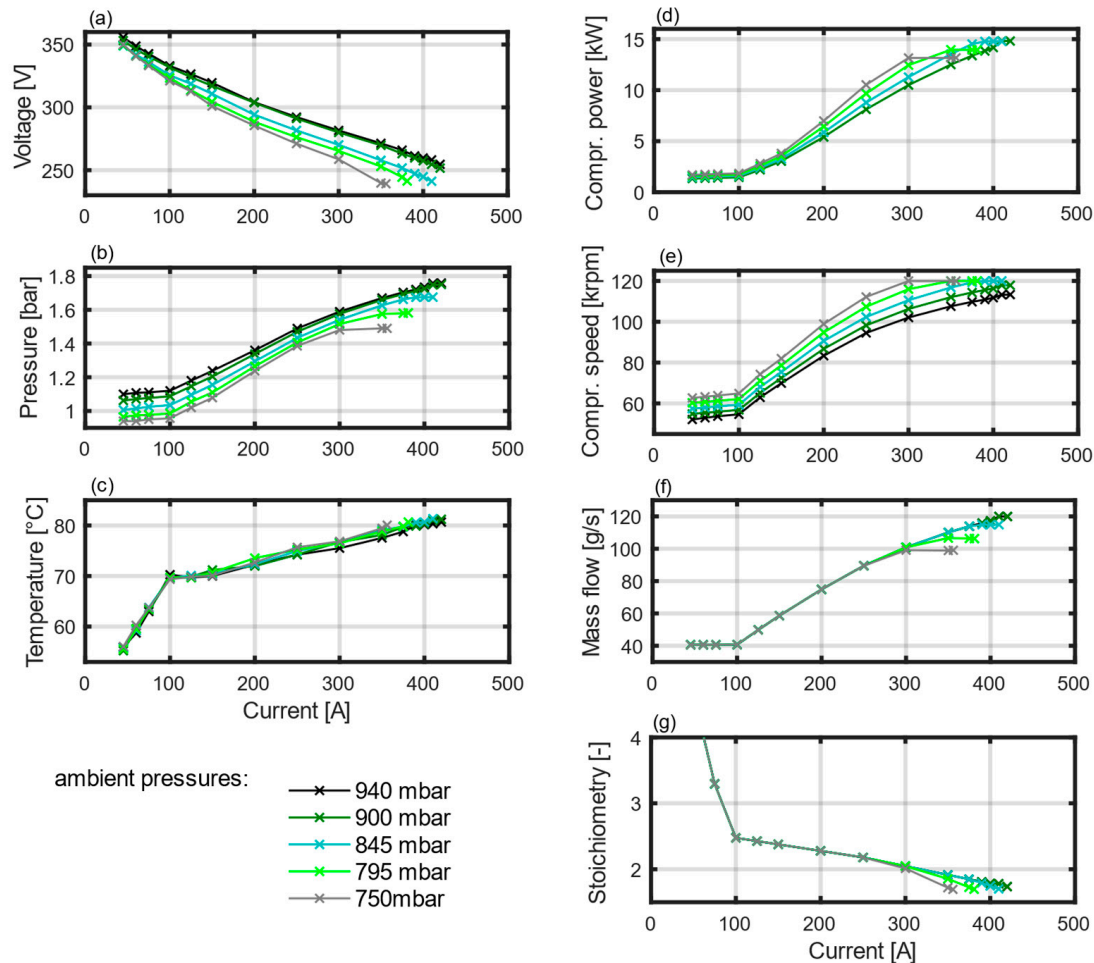

Figure 7. Current–voltage characteristics (**a**) as well as cathode inlet pressure (**b**), fuel cell outlet temperature (**c**), compressor power (**d**), compressor speed (**e**), air mass flow (**f**) and cathode stoichiometry (**g**) for measurements taken at various ambient pressure levels of the fuel cell system.

When looking at the fuel cell outlet temperatures and the temperature development along the varying current in Figure 7, it can be observed that the difference between the measurements at different pressures is below 3 K for all currents. It can, therefore, be concluded that the internal cooling circuit of the fuel cell system keeps the operating temperature approximately the same for operation at all ambient pressures, and the changes in performance are not due to differences in stack temperature.

The varying performance at different ambient pressures can be understood when looking at the stack inlet pressure, the compressor speed and the mass flow in Figure 7. A lower ambient pressure results in a lower stack inlet pressure. However, the compressor compensates for the lower air density by an increase in compressor speed for lower pressures, keeping the mass flow constant. Once the compressor reaches its maximum speed at 120 krpm, the compressor can no longer compensate for the lower air density, and the air mass flow decreases with lower inlet pressures at high currents, leading to a lower stoichiometry. Until the compressor's speed limit is reached, the decrease in performance of the FC is due to the lower operating pressures. Once the speed limit is reached, the reduced stoichiometry adds another effect, which reduces the fuel cell's performance.

The increase in compressor speed leads to an increase in the compressor power required at lower ambient pressures. This will lead to a lower overall power output of the FC-system if the compressor power is deducted from the stack output power. The

compressor power increases as mass flow increases but remains constant once the mass is no longer increased due to the compressor's speed limit. This is due to the fact that the power P required for the compressor depends on the mass flow, as can be observed from Equation (3), assuming isentropic compression, where $\dot{m}$ is the mass flow, κ is the isentropic exponent and R_s the specific gas constant, T_{in} the air inlet temperature, p_{out} and p_{in} the outlet and inlet pressures, M the torque and ω the rotational speed:

$$P = \dot{m} \times R_s \times T_{in} \frac{\kappa}{\kappa - 1} \left(\left(\frac{p_{out}}{p_{in}} \right)^{\frac{\kappa - 1}{\kappa}} - 1 \right) = M \times \omega \qquad (3)$$

The results show that the FC-system, which was developed for operation on the ground, can be operated at reduced ambient pressure if current is limited as described above. The power output in the low-pressure operation is limited, as the operational conditions are not ideal. With decreasing ambient pressure, the resulting cathode pressure and stack voltage for a given current are decreasing. Additionally, the maximum current is limited because the compressor cannot deliver sufficient mass flow at low ambient pressures and high currents.

6. Measurements at Maximum Current at Various Pressures

In addition to the current–voltage characteristics described above, another test was conducted, where the system was operated at its maximum possible current at an ambient pressure of 754 mbar. The ambient pressure was then increased in steps (754 mbar, 774 mbar, 837 mbar, 867 mbar, 900 mbar and 940 mbar). The result can be observed in Figure 8. It can be observed that, as pressure increases from 754 mbar to 867 mbar, higher currents can be obtained, while the voltage of the system decreases slightly from 238 V to 236 V. This is due to the newly implemented current-limiting strategy.
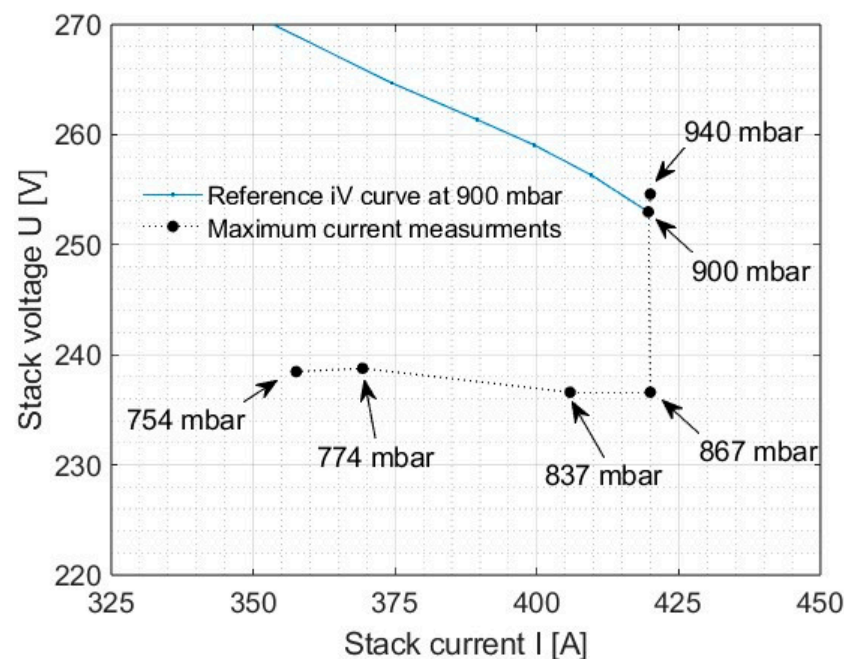

Figure 8. Operating points at the maximum possible system current for different ambient pressures with the implemented stoichiometry-dependent current limitation.

Once the ambient pressure has been increased from 754 mbar to 867 mbar, the maximum current can no longer be increased, as the limit of 420 A allowed by the system itself is reached. When the ambient pressure is increased further, the stack voltage increases, since current stays constant.

Figure 9 shows the stack power, the net power of the system, the stack voltage and current as well as the compressor speed, the airflow delivered and the stoichiometry at the maximum possible current points as shown in Figure 8. It can be observed that, for pressures below 867 mbar, the compressor speed is constant, as the speed limit of the compressor has been reached. At 867 mbar, the compressor provides almost the same air mass flow as at higher pressures, and the current is fairly constant for 867 mbar, 900 mbar and 940 mbar. However, for lower ambient pressures (837 mbar, 774 mbar, 754 mbar), the compressor can deliver less air mass flow, leading to the decrease in current that can be drawn due to the minimum stoichiometry requirements described above. The stoichiometry at 940 mbar and 900 mbar is the same, but at 867 mbar, it drops due to a slightly reduced air mass flow. The implemented current limiting keeps the stoichiometry constant for the measured pressures below 837 mbar. At the same time, the voltage varies strongly between 900 mbar and 867 mbar but remains almost constant (between 239 V and 237 V) for all pressures between 867 mbar and 754 mbar.
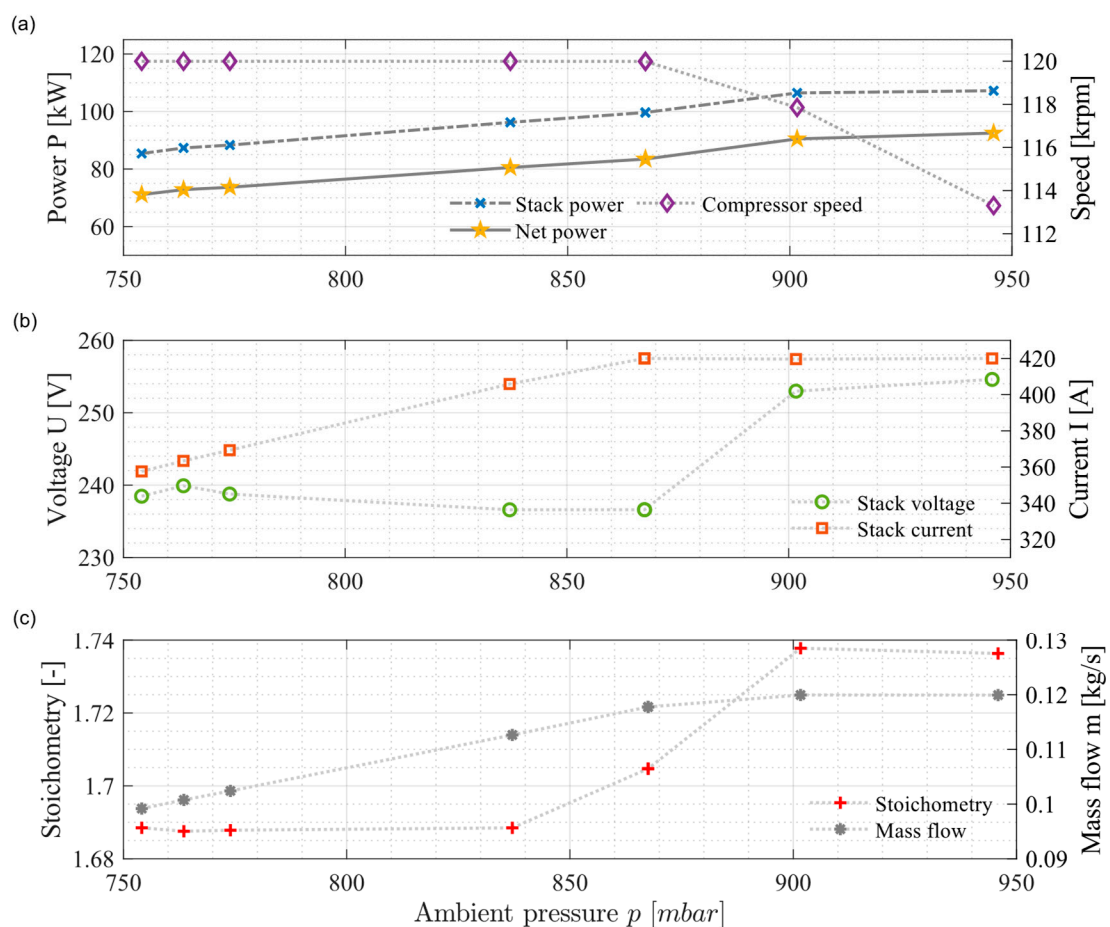

Figure 9. (**a**) Stack gross and net system power, compressor speed, (**b**) stack voltage and current, (**c**) air mass flow and cathode stoichiometry at the maximum possible current output at different altitudes.

The variations in current and voltage lead to the observed decrease in power. It can be observed in Figure 9 that the difference in stack power and net system power remains almost constant for the different ambient pressures. At 945 mbar, the difference is 14.7 kW, which corresponds to the power consumed by the compressor. This difference increases to 16.1 kW at 900 mbar, as the compressor increases its speed. At 754 mbar, the difference decreases again to 14.3 kW, despite the fact that the compressor speed remains constant. This decrease is due to the fact that the power P required for the compressor depends on the mass flow, as already described above and shown in Equation (3). In the examined system, the compressor consumes almost 17% of the stack power at an ambient pressure of

755 mbar, while it consumes only 15% at 900 mbar and 13% at 940 mbar when the system is operated at its maximum current output.

The results show clearly that the compressor in the system was chosen to meet requirements at ground operation and cannot compensate the low ambient pressure because the compressor's speed limit is reached.

To better adapt the system to the operating conditions at high altitude, the stack inlet pressure could be increased by adding a backpressure valve or turbine at the cathode exhaust outlet. This would result in higher operating pressures of the fuel cell stack and, therefore, in better performance. At the same time, a different compressor that allows for higher mass flows should be considered to avoid the drop in stoichiometry due to the speed limit of the compressor, which is described above. The mass flow for which the compressor should be designed then depends on the fuel cell system's stack requirement and the altitude for which the system is to be adapted. Note that, for adapting the FC-system to aviation applications at pressures lower than 700 mbar (higher altitudes), a change in the bearing technology of the compressor is also required, as the air bearings are limited to above 700 mbar.

7. Summary and Conclusions

A commercially available 100 kW PEM fuel cell system, originally designed for efficient ground-level operation, was tested at pressures between 750 mbar and 940 mbar. The commercial FC-system had its own control, which was not altered, but an additional test rig software was developed to enable testing at low ambient pressures. The performance of the FC-system at conditions that correspond to higher altitudes in an aviation application was then examined to assess the suitability and to identify further necessary development steps for this application.

The system was installed inside a low-pressure climate chamber. The sensibility of measurement data with respect to ambient temperature, cooling inlet temperature and ambient pressure was tested in a preliminary step to determine the necessary accuracy for the later experiments. System inlet coolant temperature had little influence on the performance of the system due to the manufacturer's own internal thermal management. The voltage variation of the system at 400 A was below 10 mV for system coolant inlet temperatures to the fuel cell system of 20 °C, 40 °C and 60 °C. The influence of the ambient temperature was found to be negligible as well. The average cell voltage of the system varied by 1.4 mV/K at 420 A for measurements at 15 °C and 20 °C. The sensitivity of the system to pressure changes was found to be 0.143 mV/mbar at 420 A and 900 mbar. To ensure reproducibility of the setup, reference I–V curves at the same reference conditions were taken, and the maximum deviation between the curves was found to be 4.65 V.

Testing at lower pressures required implementing an additional current-limiting strategy that had to be implemented into the test rig control, as the compressor could not deliver sufficient mass flow at low pressures to reach the maximum current allowed by the system (420 A), which led to a system shutdown. The newly developed current-limiting strategy reduces the current if stoichiometry falls below a user-defined threshold (set to 1.7 in the experiments). With this strategy in place, the system operated successfully at low pressures, preventing shutdowns at the expense of reduced current output. Measurements at 940 mbar, 900 mbar, 845 mbar, 795 mbar and 700 mbar ambient pressure were then performed. The temperature inside the chamber was set to 15 °C for all measurements.

The current voltage characteristics at 940 mbar and 900 mbar showed only a small difference, while the system performed visibly worse at the lower pressures of 845 mbar, 795 mbar and 700 mbar. The operating temperature at the stack was kept approximately the same for all pressure levels by the internal control of the system. As pressure decreased, the current–voltage curves were steeper, and the maximum achievable current decreased. A reduced compressor inlet pressure leads to a lower stack inlet pressure and a lower mass flow unless the compressor speed is changed. At low currents and, therefore, a lower air mass flow demand, the compressor compensated for the lower ambient air density by

increasing the compressor speed. Once the compressor reached its maximum speed, it could no longer compensate. It is, therefore, recommended to use a different compressor within the system, which allows for higher mass flows and pressure ratios, for adapting the FC-system to aviation applications. Stack inlet pressure could also be increased for operation at low ambient pressures by adding a backpressure valve or turbine at the cathode exhaust outlet.

The system's behaviour at the maximum possible current output was also examined for various pressure levels. The implemented current-limiting control strategy meant that, when ambient pressure decreases from 940 mbar to 867 mbar, the system´s maximum current remains at 420 A (the limit for the examined FC-system). The voltage decreases accordingly to the lower pressures. Below 867 mbar, however, the compressor can no longer provide a sufficient mass flow to reach 420 A, and the current is limited by the implemented current-limiting strategy. In this ambient pressure range, the voltage at the maximum output, therefore, remains constant, while the current decreases with pressure.

The measurements showed that a commercial PEM fuel cell system, which was designed for ground-level applications, can be operated at lower pressures. A necessary modification was the implementation of a current-limiting control strategy to avoid low stoichiometries that can occur when the installed compressor cannot compensate for the lower air density at high altitudes and can, therefore, not deliver sufficient air for reaching the maximum allowed current that is currently defined for the system. Another sensible modification for aviation applications would be the adaptation of the compressor hardware to enable higher mass flows and pressures at low ambient pressures to avoid having to limit the power output of the system due to the decreased air mass flow. An adaptation of the system's internal thermal management is also recommended in the future to increase the power output at low pressures and avoid potential flooding or drying of the cells.

Author Contributions: Conceptualisation, C.W., D.F., T.G., S.B. and C.B.; Methodology, D.F., S.B., T.G., S.W., C.W. and C.B.; Software, S.W.; Validation, D.F., S.B. and T.G.; Investigation, D.F., S.B. and T.G.; Data Curation, S.W., D.F., T.G. and S.B.; Writing—Original Draft, C.W. and D.F.; Writing—Review and Editing, C.W. and C.B.; Visualisation, T.G., D.F., C.W., S.B. and S.W.; Supervision, C.W. and C.B.; Project administration, C.B.; Funding acquisition, C.W. and C.B. All authors have read and agreed to the published version of the manuscript.

Data Availability Statement: The original contributions presented in this study are included in the article material. Further inquiries can be directed to the corresponding author.

Conflicts of Interest: The authors declare no conflict of interest.

References

1. Fuel Cells and Hydrogen 2 Joint Undertaking. Hydrogen-Powered Aviation: A Fact-Based Study of Hydrogen Technology, Economics, and Climate Impact by 2050. 2020. Available online: https://data.europa.eu/doi/10.2843/471510 (accessed on 17 September 2024).
2. H2FLY GmbH. H2FLY. Breaking the Hydrogen Barrier. 2022. Available online: https://www.h2fly.de/ (accessed on 29 September 2022).
3. ZeroAvia. The Clean Future of Flight. 2024. Available online: https://zeroavia.com/ (accessed on 26 October 2024).
4. AIRBUS. ZEROe. 2024. Available online: https://www.airbus.com/en/innovation/energy-transition/hydrogen/zeroe (accessed on 26 October 2024).
5. Rojas, A.C.; Lopez, G.L.; Gomez-Aguilar, J.F.; Alvarado, V.M.; Torres, C.L.S. Control of the Air Supply Subsystem in a PEMFC with Balance of Plant Simulation. *Sustainability* **2017**, *9*, 73. [CrossRef]
6. Vidović, T.; Tolj, I.; Radica, G.; Ćoko, N.B. Proton-Exchange Membrane Fuel Cell Balance of Plant and Performance Simulation for Vehicle Applications. *Energies* **2022**, *15*, 8110. [CrossRef]

7. Kamarudin, S.K.; Daud, W.R.W.; Md. Som, A.; Takriff, M.S.; Mohammad, A.W. Technical Design and Economic Evaluation of a PEM Fuel Cell System. *J. Power Sources* **2006**, *157*, 641–649. [CrossRef]

8. Willich, C.; Tomaszewski, A.; Henke, M.; Friedrich, K.A.; Kallo, J. Temperature Effect due to Internal Reforming in Pressurized SOFC. *J. Electrochem. Soc.* **2014**, *161*, F674–F678. [CrossRef]

9. Henke, M. Pressurised Solid Oxide Fuel Cells: From Electrode Electrochemistry to Hybrid Power Plant System Integration. Ph.D. Thesis, University of Stuttgart, Stuttgart, Germany, 2015. [CrossRef]

10. Atkins, P.W. *Physical Chemistry*, 5th ed.; Oxford University Press: Oxford, England, 1994.

11. Berning, T. The Dew Point Temperature as a Criterion for Optimizing the Operating Conditions of Proton Exchange Membrane Fuel Cells. *Int. J. Hydrogen Energy* **2012**, *37*, 10265–10275. [CrossRef]

12. Werner, C.; Gores, F.; Busemeyer, L.; Kallo, J.; Heitmann, S.; Griebenow, M. Characteristics of PEMFC Operation in Ambient- and Low-Pressure Environment Considering the Fuel Cell Humidification. *CEAS Aeronaut. J.* **2015**, *6*, 229–243. [CrossRef]

13. Werner, C.; Busemeyer, L.; Kallo, J. The Impact of Operating Parameters and System Architecture on the Water Management of a Multifunctional PEMFC System. *Int. J. Hydrogen Energy* **2015**, *40*, 11595–11603. [CrossRef]

14. Filsinger, D.; Kuwata, G.; Ikeya, N. Tailored Centrifugal Turbomachinery for Electric Fuel Cell Turbocharger. *Int. J. Rotating Mach.* **2021**, *2021*, 1–14. [CrossRef]

15. Lück, S.; Wittmann, T.; Göing, J.; Bode, C.; Friedrichs, J. Impact of Condensation on the System Performance of a Fuel Cell Turbocharger. *Machines* **2022**, *10*, 59. [CrossRef]

16. Antivachis, M.; Dietz, F.; Zwyssig, C.; Bortis, D.; Kolar, J.W. Novel High-Speed Turbo Compressor with Integrated Inverter for Fuel Cell Air Supply. *Front. Mech. Eng.* **2021**, *6*, 612301. [CrossRef]

17. Toyota Industries Corporation. Toyota Industries Develops New FC Air Compressor and Hydrogen Circulation Pump, Now Installed in the New Toyota Mirai FCEV. 2020. Available online: https://www.toyota-industries.com/news/2020/12/10/005056/index.html (accessed on 28 October 2024).

18. Schröter, J.; Frank, D.; Radke, V.; Bauer, C.; Kallo, J.; Willich, C. Influence of Low Inlet Pressure and Temperature on the Compressor Map Limits of Electrical Turbo Chargers for Airborne Fuel Cell Applications. *Energies* **2022**, *15*, 2896. [CrossRef]

19. Gravdahl, J.T.; Egeland, O. Centrifugal Compressor Surge and Speed Control. *IEEE Trans. Control Syst. Technol.* **1999**, *7*, 567–579. [CrossRef]

20. Wu, Y.; Thilges, C. Centrifugal Compressor Performance Deviations with Various Refrigerants, Impeller Sizes and Shaft Speeds. 2014. Available online: https://docs.lib.purdue.edu/icec/2286/ (accessed on 22 October 2024).

21. Schröter, J.; Steinbarth, D.; Bauer, C.; Reichmann, U.; Kallo, J.; Willich, C. Climate and Pressure Chamber for Simulation of Flight Conditions. 2021. Available online: https://doi.org/10.18725/OPARU-38012 (accessed on 17 September 2024).

22. PowerCell Group. Hydrogen Fuel Cell Systems, Power Generation System 100. Available online: https://powercellgroup.com/fuel-cell-systems/ (accessed on 25 September 2024).

23. O'Hayre, R.; Cha, S.-W.; Colella, W.; Prinz, F.B. *Fuel Cell Fundamentals*, 1st ed.; John Wiley & Sons, Inc.: Hoboken, NJ, USA, 2016. [CrossRef]